Nanoscale

PAPER

View Article Online
View Journal | View Issue

Cite this: *Nanoscale*, 2024, **16**, 3144

Ion transport mechanisms in pectin-containing EC–LiTFSI electrolytes†

Sipra Mohapatra,[a] Hema Teherpuria,[a] Sapta Sindhu Paul Chowdhury,[a] Suleman Jalilahmad Ansari,[a] Prabhat K. Jaiswal,[a] Roland R. Netz[b] and Santosh Mogurampelly *[a,b]

Received 11th August 2023,
Accepted 5th January 2024

DOI: 10.1039/d3nr04029a

rsc.li/nanoscale

Using all-atom molecular dynamics simulations, we report the structure and ion transport characteristics of a new class of solid polymer electrolytes that contain the biodegradable and mechanically stable biopolymer pectin. We used highly conducting ethylene carbonate (EC) as a solvent for simulating lithium–trifluoromethanesulfonimide (LiTFSI) salt containing different weight percentages of pectin. Our simulations reveal that the pectin chains reduce the coordination number of lithium ions around their counterions (and *vice versa*) because of stronger lithium–pectin interactions compared to lithium–TFSI interactions. Furthermore, the pectin is found to promote smaller ionic aggregates over larger ones, in contrast to the results typically reported for liquid and polymer electrolytes. We observed that the loading of pectin in EC–LiTFSI electrolytes increases their viscosity (η) and relaxation timescales (τ_c), indicating higher mechanical stability, and, consequently, a decrease of the mean squared displacement, diffusion coefficient (D), and Nernst–Einstein conductivity (σ_{NE}). Interestingly, while the lithium diffusivities are related to the ion-pair relaxation timescales as $D_+ \sim \tau_c^{-3.1}$, the $TFSI^-$ diffusivities exhibit excellent correlations with ion-pair relaxation timescales as $D_- \sim \tau_c^{-0.95}$. On the other hand, the NE conductivities are dictated by distinct transport mechanisms and scales with ion-pair relaxation timescales as $\sigma_{NE} \sim \tau_c^{-1.85}$.

Introduction

The nature of the electrolyte material sandwiched between the electrodes in a rechargeable battery device is critical for developing advanced lithium-ion batteries that are safe, lightweight, durable, and mechanically stable.[1–4] Among different classes of electrolyte materials, solid polymer electrolytes (SPEs) are generally preferred due to their several advantages.[2,4,5] Explicitly, SPEs outperform the traditionally used liquid electrolytes in providing safety, a better solid electrolyte interface, and better mechanical stability to batteries by stopping dendrite growth.[6–9] SPEs also serve as a better choice over liquid electrolytes due to their high mechanical stability, ease of processing, and negligible interfacial resistance.[1,10] Accordingly, significant efforts have been focused on addressing some critical issues associated with SPEs, including their low ionic conductivity at room temperature in fully commercializing SPE-based battery technologies. Researchers have made significant efforts in achieving high energy density requirements of electrolytes for battery applications by enhancing their ionic conductivity.[11–13]

Besides increasing the ionic conductivity, developing advanced electrolyte materials, which are also biocompatible, holds promise for future battery technologies. Due to their solid nature, biocompatible solid electrolytes have the significant advantage of being chemically stable and have minor safety issues.[14,15] In this context, researchers are actively exploring advanced SPEs based on naturally occurring biopolymers instead of synthetic polymers (such as PEO) due to the promise of environmental compatibility owing to their biodegradable nature.[16–19] Naturally occurring polymers are mainly composed of repeated monomeric units of saccharides, fatty acids, amino acids, and nucleotides and are primarily found in biological organisms.[20,21] Polysaccharides are natural biopolymers made of carbohydrate monosaccharides linked through *o*-glycosidic linkages. Biopolymers such as starch,

[a]*Department of Physics, Indian Institute of Technology Jodhpur, N.H. 62, Nagaur Road, Karwar, Jodhpur, Rajasthan 342030, India. E-mail: santosh@iitj.ac.in*
[b]*Fachbereich Physik, Freie Universität Berlin, 14195 Berlin, Germany*

†Electronic supplementary information (ESI) available: It contains (S1) the visual impression of the simulated systems, (S1.1) the force field parameters for the pectin polymer (Table ST1: bonded and non-bonded force field parameters for the pectin polymer and Table ST2: system details), (S2) the radial distribution function and coordination number, (S3) ion association probability, (S4) mean squared displacement (Table ST3: diffusion coefficient calculations from the MSD curves), (S5) calculation of viscosity and notes on numerical issues, (S6) diffusion coefficient scaling with η and τ_c, (S7) the ion-pair correlation function, (S8) pectin loading dependency of σ_{NE}, η, $P(0)$, $P(1)$ and $P(2)$ and an intuitive objective function $f(\sigma_{NE}, P(0), P(1)) \sim \sigma_{NE}P^a(0)/P^b(1)$, and (S9) the transference number with wt% of pectin. See DOI: https://doi.org/10.1039/d3nr04029a

chitosan, agar–agar, cellulose, *etc*. previously have been proposed as polymer hosts in battery electrolytes.[18,22–24] In the past decade, significant progress has been made in improving the properties of biocompatible electrolyte materials for battery applications. For instance, biodegradable gel polymer electrolytes developed by Gou *et al.* showed stable capacity retention, minimal fading, and high coulombic efficiency.[25] Lin *et al.* designed biocompatible electrolytes using corn starch in a PEO–LiTFSI system with different wt%s of corn starch.[26] They observed an increase in the ionic conductivity of the composite electrolyte with the loading of corn starch and the highest conductivity of 2.62×10^{-5} S cm^{-1} at a ratio of PEO : corn starch = 9 : 1. Biocompatible SPEs developed by Zhou *et al.* are stretchable and flexible with a self-healing nature that can be crucial in battery applications.[27] For the commercial adoption of biocompatible SPEs in batteries, their ionic conductivity should be comparable to that of liquid electrolytes. However, the ionic conductivity of biocompatible electrolytes is typically much lower than that of liquid electrolytes (10^{-2} to 10^{-3} S cm^{-1}),[8,28] which remains a significant challenge for their applications. Since the ionic conductivity of polymer-based electrolytes is highly dependent on the ion-solvating capabilities of the host polymer matrix, the choice of biopolymers is critical for developing efficient battery electrolyte materials. The choice of salts for pectin–EC electrolytes is crucial for achieving higher ionic conductivity in lithium-ion batteries. Traditional lithium salts such as $LiClO_4$, $LiPF_6$, $LiAsF_4$, and $LiBF_4$ strongly aggregate in many solvents. The ion aggregation depends on the salt concentration and temperature, but the size of the ion also matters for the faster movement of counterions. The delocalization of charge over a larger molecular ion such as TFSI (in LiTFSI salt) can facilitate faster movement of counterions due to the less ion–ion correlations and strong Li–polymer coordination,[9,29,30] which contributes to the ionic conductivity of the electrolytes. Apart from that, LiTFSI is known for its high chemical and thermal stability, which is crucial for the performance and safety of lithium-ion batteries.

Pectin ($C_6H_{10}O_7$), a polysaccharide biomacromolecule consisting of α-1,4-linked D-galacturonic acid monomers, is highly abundant in nature and typically found in the cell walls of plants, fruit extracts, and agricultural products.[24,31] Pectin plays a key role in maintaining the cell wall structure and provides rigidity to plants and fruits. Furthermore, pectin indirectly helps in regulating the permeability of water, nutrients, and other small molecules in the biological environment. Some environmental advantages of using pectin in technological applications include its polysaccharide nature, ease of fabrication, and ultralow toxicity.[23] Considering these intriguing features, we propose to integrate pectin with traditional highly conducting liquid electrolytes for the development of advanced solid-state battery electrolyte technologies. Besides possessing the desired solvating capabilities and environmental advantages, different functional groups on monomers can result in a variety of structural complexities of pectin that are likely to offer exciting consequences for ion transport. One of the possible outcomes of flexibility in choosing different monomeric architectures is pectin-based SPEs with unique ion transport characteristics similar to those reported for single-ion conductors and/or polymeric ionic liquid electrolytes.[32,33] The anionic nature of the monomeric polysaccharide unit enables ionic coordination with the surrounding cations present in the electrolyte material, similar to polyelectrolytes,[34–36] and may promote efficient ion transport.[28] Motivated by the above-discussed issues, we proposed pectin biomacromolecules for developing pectin-based SPEs as alternatives to synthetic polymer-based SPEs and investigated their structure and ion transport properties.

There are only a few experimental studies on pectin-based electrolytes in the literature. In 2009, J. R. Andrade *et al.* prepared a transparent gel electrolyte composed of methanol-esterified pectin chains and glycerol as a plasticizer with $LiClO_4$ salt.[37] They observed the ionic conductivity of a methanol-esterified pectin-based glycerol–$LiClO_4$ gel bio-polymer electrolyte to be 4.7×10^{-4} S cm^{-1} with 68 wt% of glycerol at room temperature. Perumal *et al.*, in their experimental work,[38] found that an electrolyte composed of equal molecular wt% of pectin and LiCl offered an ionic conductivity of 1.96×10^{-3} S cm^{-1}, which is higher than that of a $LiClO_4$-(40 wt% $LiClO_4$ + 60 wt% pectin) incorporated electrolyte with an ionic conductivity of 5.38×10^{-5} S cm^{-1}. A thorough understanding of the structural properties, underlying transport mechanisms, and mechanical stability of pectin-based SPEs is still required to develop an alternative to traditionally used electrolytes.

In this work, we investigated the effect of pectin loading on the transport and structural properties of typical commercial EC–LiTFSI battery electrolytes using atomistic simulations. The ion structure was investigated to study the ion-solvating capability of pectin, which is a crucial factor for the transportation of ions in electrolytes. The radial distribution function ($g(r)$), coordination number (CN(r)), and ion association probability ($P(n)$) were investigated to study the structural compactness and intermolecular interactions between the ion–ion, ion–polymer, and ion–solvent. The underlying ion transport mechanism was quantified through the ion-pair relaxation time (τ_c) and the diffusion coefficients (D) of the Li cation and the TFSI anion. Furthermore, we calculated the Nernst–Einstein ionic conductivity and viscosity (η) to understand the ionic transport behavior and mechanical stability. Finally, before summarizing the main results of our simulations, we provide insights into the implications of the validity and breakdown of the diffusivity power-law relationship $D \sim {\tau_c}^{-1}$ and discuss the choice of optimal loading of pectin in maximizing the benefits of pectin in the context of ionic conductivity and mechanical stability of the pectin–EC–LiTFSI electrolyte systems. There are several advantages and disadvantages of using pectin in battery applications. Based on the prospects of pectin and the key outcomes of this work, we summarize here some of the major advantages of pectin-containing electrolytes: (i) the addition of pectin increases the mechanical stability of the electrolytes, which is currently one of the major issues associated with the commercially available liquid elec-

trolytes, (ii) pectin makes the battery electrolytes biodegradable to a large extent, (iii) pectin reduces the larger ionic clusters and promotes the smaller ionic clusters, which can help in improving the ionic conductivity of the electrolytes, and (iv) pectin is a biopolymer and abundant in nature, which can make the battery electrolytes cost-effective. On the other hand, the major disadvantages of pectin-containing electrolytes are: (i) the diffusivity of monoatomic ions like Li ions decreases significantly with pectin, (ii) the ionic conductivity is expected to decrease with higher pectin loading, which is not favorable for battery applications; however, this can be circumvented with electrolyte design strategies, and (iii) monoatomic ions and smaller molecular ions are highly likely to be trapped by pectin in its backbone.

Simulation methods

Interaction potential model and force fields for pectin and EC–LiTFSI electrolytes

We performed all-atom molecular dynamics simulations of pectin–EC–LiTFSI electrolytes at different loading of pectin using the GROMACS 2021.2 package[39,40] with the following interaction potential:

$$U(r) = U^{\text{bonded}}(r) + \sum 4\varepsilon\left[\left(\frac{\sigma}{r_{ij}}\right)^{12} - \left(\frac{\sigma}{r_{ij}}\right)^{6}\right] + \sum \frac{q_1 q_2}{4\pi\varepsilon_0 r_{ij}} \quad (1)$$

In the above equation, the U^{bonded} includes all the intramolecular interactions with contributions from bonds, angles, and torsions. The remaining terms correspond to the non-bonded interactions and are modeled with the Lennard-Jones interaction potential and the Coulomb potential. A scaling factor of 0.5 was used for the non-bonded interactions between intramolecular atomic pairs separated by three bonds. The scaling factor, however, was not used for the intramolecular atomic pairs separated by more than three bonds. A real space cutoff of 12 Å was used for the LJ and Coulomb interactions, and *k*-space summation for the electrostatic interactions was carried out using the particle mesh Ewald method.[41] The LJ interactions beyond the cutoff distance were truncated by including analytical tail corrections for pressure and energy.

The force field parameters for EC and LiTFSI salt were extracted from the standard optimized potential for the liquid simulation-all-atom (OPLS-AA) force field set developed by Jorgensen[42] with improved intramolecular parameters from Acevedo.[43] The total charge on ionic species was scaled to 0.8*e* to indirectly mimic the induced polarization effects in a mean field-like manner.[44] This approach was previously shown to produce results compared to polarizable models and experiments.[45–49] The OPLS-AA parameter set produces good results for the structure and diffusion coefficient of ions in neat EC–LiTFSI electrolytes, consistent with experiments.[5,50] The LJ non-bonded parameters for all atomic types in pectin are taken from the GLYCAM06J parameter set[51] suitable for polysaccharides. Among different esterification states of pectin [depending on the extraction from agricultural products and possessing different properties], we considered the COOH esterification on its monomers. Therefore, the intramolecular interaction parameters (excluding the dihedral angles) and partial atomic charges of pectin were obtained in this paper by performing quantum mechanical calculations, as explained in the following section. The Lorentz–Berthelot arithmetic rules were followed to calculate the non-bonded parameters for the cross-interaction terms between different atom types of pectin. However, to be consistent with the OPLS-AA force field, the cross-interaction terms between different atomic types of EC–LiTFSI were calculated using the geometric mixing rules. Similarly, the cross-terms between pectin and EC–LiTFSI were also calculated using the geometric mixing rules.

Development of the intramolecular force field parameters for pectin

Quantum mechanical calculations were performed to generate the force field parameters by simulating the monomer of pectin using density functional theory (DFT) with the B3LYP/6-311g** basis set[52,53] using the Gaussian16 package.[54] We have optimized the geometry of a monomeric unit of pectin to calculate the equilibrium bond lengths and angles in pectin.[55] The normal mode analysis of equilibrium vibrational frequencies was performed to estimate the force constants of harmonic potentials for all bonds and angles. The partial atomic charge of all atomic types of pectin was evaluated by fitting the electrostatic potential to atomic centers using the RESP fitting method.[56] The parameters of equilibrium dihedral torsion angles and the respective force constants were taken from the GLYCAM06J parameter set.[51] The complete force field parameters are provided in Table ST1 in the ESI.†

Initial system setup

The molecular structure of the pectin chain was generated using GLYCAM oligobuilder software, consisting of 12 monomeric units.[51] The chemical composition of the monomeric unit is the 1,4-α linkage of D-galacturonic acid (OH–$[C_6H_{10}O_7]_n$–OH),[24] and the polymer chain was terminated with a hydroxyl group. The pectin biopolymer is a class of wall polysaccharides with a complex structure. According to their functionality, various pectin structures are available, like homogalacturonan and rhamnogalacturonan acidic polymers. Esterification attaches an ester (R–OOH) group to the pectin chain. A homogalacturonan is a linear combination of D-galacturonic acid with a 1,4 alpha linkage, which we have used to investigate the movement of ions in a liquid-based system.[57]

The initial configuration of the electrolyte system was then prepared by randomly placing 5240 EC molecules in the simulation box using PACKMOL.[58] The EC system was then solvated with 100 Li^+ and 100 $TFSI^-$ ions to maintain an approximately constant salt concentration for the LiTFSI salt in all the electrolytes studied in this paper. The molar concentration of the pectin–EC–LiTFSI electrolytes simulated in this work is 0.3 M, approximately constant at all the wt% of pectin. Several recent

works have highlighted that electrolytes with high salt concentrations close to 1 M may offer optimal performance for battery applications.[59–62] However, our choice of a lower concentration in this work is motivated by the need to mitigate simulation issues associated with a high salt concentration, such as increased ion–ion correlations and high viscosity. Electrolytes with higher concentrations have not been extensively explored due to issues with efficient ionic conductivity, as an increased salt concentration leads to inefficient ionic conductivity. To prepare different composite electrolyte systems with varying wt%s of pectin, we added appropriate numbers of pectin chains in the simulation box. We prepared 8 different composite electrolyte systems with pectin wt%s of 0.5, 1, 2, 3, 5, 10, 30, and 50, along with the neat EC–LiTFSI (0 wt%). The initial system with a tolerance of 2 Å between any two atoms was prepared. Furthermore, such a low density was chosen to ensure that the electrolyte systems do not suffer potential energy traps, leading to numerical instabilities arising from the close contacts between different atoms or molecules. Details of the number of atoms, volume, density, *etc*., of different pectin wt%s in the EC–LiTFSI systems at 425 K are reported in Table ST2 in the ESI.†

Equilibration protocol

Minimization was performed on the systems consisting of pectin with different wt%s solvated with suitable numbers of Li^+ cations and $TFSI^-$ anions and EC molecules. The PACKMOL[58] generated structures containing pectin, EC, and LiTFSI were minimized using the steepest descent method for 1000 steps with a tolerance of 10 kJ mol^{-1} nm^{-1} on forces. The energy-minimized systems were then subjected to an NVT ensemble using a V-rescale[63] thermostat for 100 ps with a 1 fs step size and subsequently subjected to a 10 ns NPT ensemble with a V-rescale thermostat and a Berendsen barostat[64] with a time step of 1 fs at 425 K. Damping relaxation times of 0.1 ps and 2 ps were used in the thermostat and barostat, respectively. A compressibility factor 4.5×10^{-5} bar^{-1} was used for the NPT ensemble. Bond lengths involving hydrogen atoms were constrained to their equilibrium lengths using the LINCS algorithm.[65] The equations of motion were integrated using the leapfrog algorithm with a simulation time step of 2 fs,[66] and the trajectories were saved every 1 ps. A representative snapshot of pectin–EC–LiTFSI electrolytes at 30 wt% is shown in Fig. S1† to give a visual impression.

As discussed above, the equilibration protocol consists of initial minimization, then a short NVT, and finally, the density equilibration with an NPT ensemble. After attaining the equilibrium, the simulated density of the neat electrolyte (EC–LiTFSI, EC : Li = 48 : 1, 425 K) was obtained to be 1186 ± 5 kg m^{-3}, comparable to that obtained from experiments.[59,60,67] We generated 300 ns long production trajectories at different wt% s of pectin in the NPT ensemble, among which the last 50 ns was used for analyzing the structural properties (such as $g(r)$, CN(r), and $P(n)$), and the entire trajectory was used for analyzing the transport and relaxation phenomena (such as MSDs, D, τ_c, and σ_{NE}). For viscosity calculations, we performed 50 independent *NPT* runs of 1 ns with a finer resolution saving frequency of 1 fs to calculate the pressure tensor autocorrelation function.

Results and discussion

Here, we discuss the structural and transport properties of pectin and ions in pectin–EC–LiTFSI electrolytes. The ion diffusion coefficients were compared with ion-pair relaxation timescales to understand the underlying ion transport mechanisms.

Ion density profiles

As discussed in the Introduction section, we propose/hypothesize that pectin possesses good ion-solvating capabilities for its applications in lithium-ion batteries. To examine the nature of ion-solvating features of pectin, we calculated the density profiles of different ionic species in pectin-loaded EC–LiTFSI electrolytes in the x, y, and z directions. As shown in Fig. 1, for the neat EC–LiTFSI system (0 wt%, bottom subplot), we confirmed the uniform distribution of Li^+ and $TFSI^-$ ions in the electrolyte. This result establishes that EC is an excellent solvent for uniformly dissolving LiTFSI salt without the formation of large ionic clusters or aggregates. With the addition of pectin to the EC–LiTFSI electrolytes, the uniformity of the distribution of ionic species is not significantly affected. Still, the distribution of ionic species appears to fluctuate, which monotonically increases with the loading of pectin. Interestingly, these fluctuations are uniform across the simulation box, confirming that pectin does not induce the formation of ionic clusters or aggregates, similar to the neat EC–LiTFSI electrolytes. The fluctuations at a higher loading of pectin are expected because of the electronegative charge groups on the backbone of pectin. The above results suggest that no ionic clusters are formed in the presence of pectin, supporting the suitability of pectin for battery electrolyte applications and the possibility of the desired ion conducting capabilities of pectin.

Radial distribution functions and association probability

Apart from the ion-solvating capabilities, the uniform distribution of ionic species and associated fluctuations also indicates the abundance of strong ion–ion and ion–polymer interactions.[68] To understand the structural arrangement of the pectin–EC electrolytes, we calculated the radial distribution functions, $g(r)$, between different atomic species of ion–ion and ion–polymer interactions and the respective coordination numbers, CN(r). Fig. 2(a) and (b) display the $g(r)$ and CN(r) between the anionic and cationic pairs. We observed the first peak and first minima at distances of 4.25 Å and 5 Å, respectively. However, a monotonic but rapid decrease in the first peak is observed with the loading of pectin chains. Similarly, despite a moderate increase in the number density of ions with pectin, the corresponding coordination number decreases significantly with the loading of pectin at the first peak and

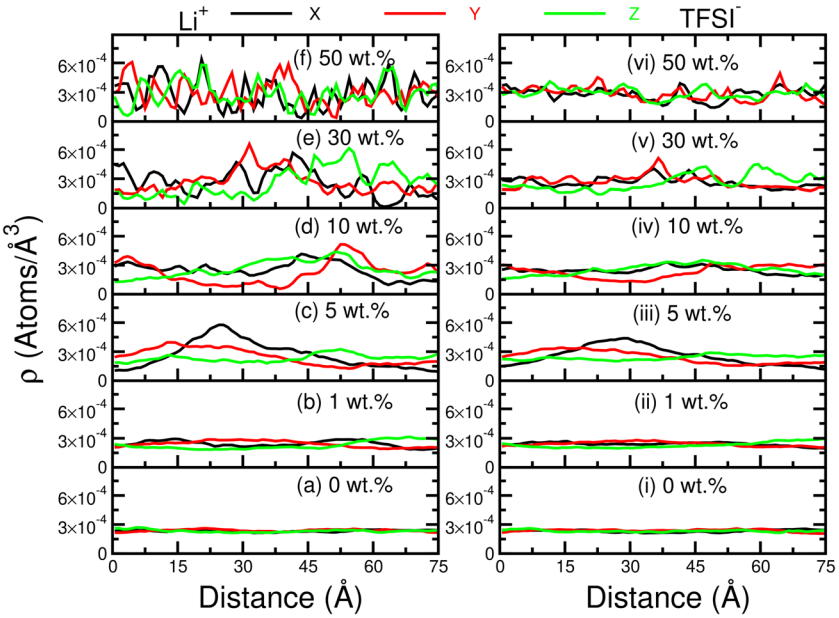

Fig. 1 Number density profiles of Li^+ and $TFSI^-$ ions in pectin-loaded systems at different wt%s along the *x*, *y*, and *z* axes.

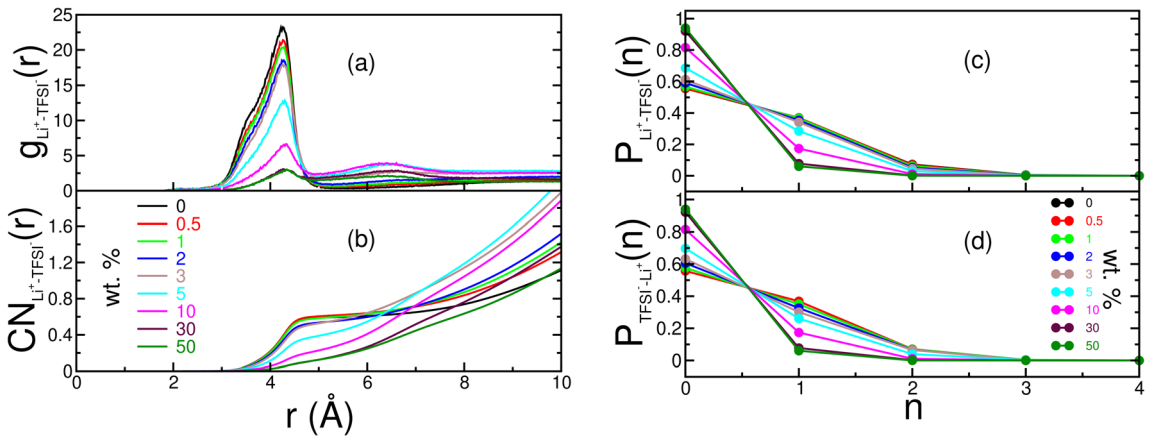

Fig. 2 (a) Radial distribution function of Li–TFSI ionic pairs, (b) coordination number of $TFSI^-$ ions around Li^+ ions, and the ion association probability of (c) finding *n* number of $TFSI^-$ ions around Li^+ ions and (d) finding *n* number of Li^+ ions around $TFSI^-$ ions.

slightly up to a larger extent beyond the first coordination shell (see Fig. S2 in the ESI†). These results indicate that the ion-pair coordination in neat EC–LiTFSI electrolytes is relatively strong despite their high ionic conducting properties. Furthermore, the monotonic decrease of ion-pair coordination with pectin loading suggests that pectin can facilitate efficient ionic conductivity compared to electrolyte systems dominated by strong ion-pair correlations.[69] Specifically, the reduced ion–ion correlations contribute to a high ionic charge carried by a given ion. Since the salt concentration in our work is 0.3 M, it is possible to increase ionic conductivity by simply increasing it beyond 0.3 M at the expense of efficient ionic conductivity due to the increased ion–ion correlations at high salt concentrations.[60,61] Apart from increasing the salt concentration to enhance the overall ionic conductivity of the pectin–EC–LiTFSI electrolytes, it is also possible to employ well-known strategies such as tuning the pectin content using an intuitive objective function [as discussed later in this paper], using plasticizers, using a different solvent instead of EC, and nanofillers for improving overall ion transport for practical applications. Despite the strong nature of ion–ion interactions, the CN(*r*) reveals that roughly half an anion (~0.6 numbers of $TFSI^-$ ions) is coordinated around cations within the first coordination shell in neat EC–LiTFSI electrolytes, consistent with previous calculations, which further reduced with the loading of pectin.

For a detailed understanding of the probability of either free ion formation or *n* number of ion coordinations around

their counterions, we calculated the ion association statistics, ($P(n)$), and show the results in Fig. 2(c) and (d). The ion association probability was calculated using

$$P(n) = \frac{1}{N_{\text{frames}}} \sum_{i=1}^{N_{\text{frames}}} \sum_{j=1}^{N_{\text{ions}}} \frac{\delta_{n_i n_j}}{N_{\text{ions}}} \quad (2)$$

where $\delta_{n_i n_j}$ is the Kronecker delta function to count n number of counterions within the first coordination shell of ion j, N_{ions} is the total number of ions, and N_{frames} is the total number of frames. Here, $\delta_{n_i n_j}$ is defined in such a way that $\delta_{n_i n_j} = 1$ if the n_ith ion is found within the first coordination shell of the n_jth ion, and $\delta_{n_i n_j} = 0$ otherwise. Consistent with $g(r)$ and CN(r), the probability of finding free ions increases with pectin loading (see Fig. 2(c), (d) and Table 1). Consequently, the probability of association with n = 1 or 2 ions around their counterions decreases with pectin loading. The increase of free ions and the decrease of ionic aggregates are characteristic effects of pectin in the electrolyte, considering that the salt concentration of the electrolyte increases with the loading of pectin (see Table 1). The densely packed solvation environment of ions in the electrolyte intuitively results in large ionic aggregates, but in contrast to intuition, pectin distracts such ionic associations by attracting cations towards the pectin backbone (see next paragraph). The decrease of ionic aggregation at a high loading of pectin indicates a large potential of pectin in positively influencing the ionic conductivity of pectin–EC–LiTFSI electrolyte systems.[59] Therefore, the presence of pectin chains helps in decoupling the ion–ion correlations that would promote efficient ionic conductivity. However, a deeper analysis of different types of ionic aggregates beyond the association probabilities (*i.e.*, aggregates of more than 1 cation and more than 1 anion simultaneously) is required to gain a better understanding of the ionic conductivity.[70]

The $g(r)$ and CN(r) associated with different atomic pairs representing the ion–polymer and polymer–polymer interactions are provided in the ESI (Fig. S2†). The ion association probabilities of other important atomic species are shown in Fig. S3 in the ESI.† Briefly, these results indicate strong polymer–polymer interactions and polymer–cation interactions in the pectin–EC electrolytes. Consistent with the decreased cation–anion interactions, we found intriguing observations for the lithium–EC and lithium–pectin interactions as observed from CN(r) and $P(n)$ as shown in Fig. S2 and S3.† Similar to the number of anions around cations, the number of EC molecules around cations also decreases within the first coordination shell as pectin loading increases. A similar observation was made for the number of EC molecules around anions. Since pectin chains accommodate cations on its backbone, the number of oxygen atoms increases with the loading of pectin. The implications of these results on ion transport and viscosity are discussed in the following sections.

Table 1 Ion association probabilities of finding n number of $TFSI^-$ ions around Li^+ ions, $P(n)$ at n = 0 and n = 1, the normalized ionic number density (ρ/ρ_0), and the normalized volume (V/V_0) with respect to the pectin-free neat EC–LiTFSI electrolyte

wt%	$P(0)$	$P(1)$	ρ/ρ_0	V/V_0
0	0.56	0.37	1.000	1.000
0.5	0.56	0.37	1.005	0.995
1	0.57	0.37	1.007	0.993
2	0.59	0.35	1.010	0.990
3	0.61	0.34	1.014	0.987
5	0.69	0.28	1.020	0.980
10	0.82	0.17	1.037	0.965
30	0.92	0.08	1.107	0.903
50	0.94	0.06	1.190	0.840

Mean squared displacement and diffusion coefficient

The present work is based on the hypothesis that the involvement of the pectin matrix can affect the ion conductivity and mechanical stability of SPEs. To clarify this, we have calculated the mean squared displacement to study the ion transport properties of both cations and anions. The self-diffusion coefficient can help us to understand ion transport characteristics, and the diffusion coefficient can be determined from the mean squared displacement (MSD). We have calculated the MSD for both Li^+ and $TFSI^-$ ions from,

$$\text{MSD}(t) = \frac{1}{N_{\text{frames}} - t} \sum_{t'=0}^{N_{\text{frames}}-t} \frac{1}{N} \sum_{i=1}^{N} \left[\vec{r}_i(t+t') - \vec{r}_i(t')\right]^2 \quad (3)$$

where N is the number of atoms and $\vec{r}_i$ is the position vector. The results shown in Fig. 3(a) indicate that lithium ions remain in the sub-diffusive region up to an order of 10^4 ps. A clear diffusive regime is observed at timescales beyond 100 ns for lower wt%. The extent of the sub-diffusive regime and the onset of the diffusive regime increase with the loading of pectin. Interestingly, the $TFSI^-$ ions show higher mean squared displacements than lithium ions, with the distinction being more pronounced at higher loading. Since the $TFSI^-$ ions are larger molecular ionic species than lithium ions, we propose that a loosely packed solvation shell formed due to the delocalized ionic charge distribution around $TFSI^-$ ions helps them display higher MSDs in relation to lithium ions, inspired by the recent works of Olvera de la Cruz[71] and Hall.[29] However, while we do not have clear evidence for the correlation between ion diffusion and its size, there is still a debate on whether the size of an ion has a direct connection with the ionic diffusivity.[72,73] As seen in Fig. 3(a), we observed that MSDs decrease with pectin loading with implications for the diffusion coefficient of ions, which was calculated as $D = \lim_{t\to\infty} D^{\text{app}}(t) = \lim_{t\to\infty} \frac{\text{MSD}(t)}{6t}$, where $D^{\text{app}}(t)$ is the time-dependent apparent diffusion coefficient calculated from the diffusive regime of MSD curves (see Fig. 3(b)). In Table ST3 of the ESI,† we provided the details of the time period over which the MSD curves were fitted to calculate the diffusion coefficient of ions and the diffusion exponent as in the $\text{MSD}(t) \sim t^{\lambda}$ obtained from the apparent linear regime.

In Fig. 4, we displayed the diffusion coefficient of the cations and anions as a function of loadings of the pectin

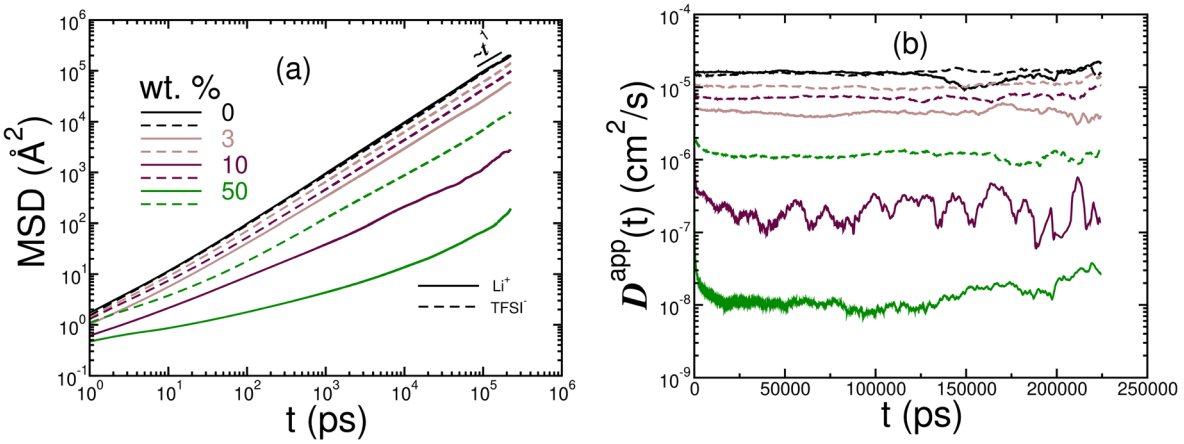

Fig. 3 (a) MSDs of Li^+ and $TFSI^-$ ions at selected values of pectin loading, *i.e.*, 0, 3, 10, and 50 wt% loadings of pectin chains. The $TFSI^-$ ions show higher MSD than the Li^+ ions. (b) The apparent diffusion coefficient as a function of lag time at different wt%s of pectin loading (legends are the same as Fig. 3(a)).

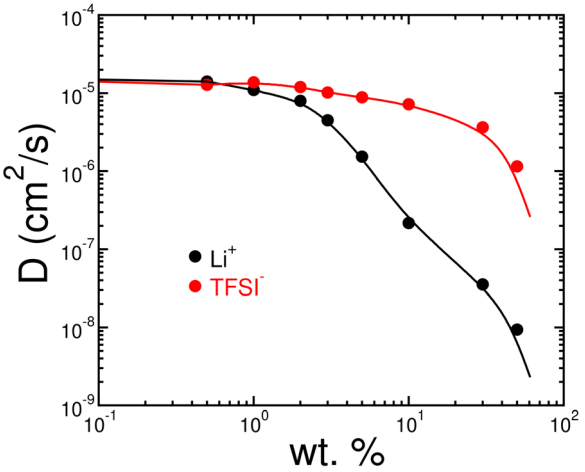

Fig. 4 Diffusion coefficients of Li^+ and $TFSI^-$ ions as a function of the wt% of pectin in EC–LiTFSI electrolytes. The solid lines are spline fits meant to guide the eye.

chains. Because pectin is a highly viscous material, the diffusion coefficient of ions is expected to decrease, and the effect increases with an increase in the loading of pectin. Consistently, we found that the diffusion coefficient of ions decreases in the presence of pectin. In addition to the viscous nature of pectin, the decrease in diffusion coefficient is also consistent with the increased ion concentration at higher loadings of pectin. The diffusion coefficient of $TFSI^-$ ions is higher than that of Li^+ ions, consistent with the corresponding MSD data presented in Fig. 3(a) and S4.† However, we observed an interesting trend at lower pectin content (up to 3 wt%) that the rate of change of the diffusion coefficient with pectin loading is somewhat similar for both the Li^+ and $TFSI^-$ ions. Furthermore, the diffusivity of lithium ions is more significantly affected compared to the $TFSI^-$ ions. The decay rate in the diffusivity of Li^+ ions is substantially faster than that of $TFSI^-$ ions, indicating a decrease in the total ionic conductivity. As a monatomic ion, lithium has more tendency to interact with polymeric electronegative groups and be trapped, which explains why lithium diffusion is drastically reduced compared to the diffusion of the larger $TFSI^-$ ions. Explicitly, the ratio between the diffusion coefficients of lithium and $TFSI^-$ ions is almost 100 at higher wt%s of pectin in the electrolytes.

Viscosity and ion-pair relaxation timescales

It is known that the viscous nature of the electrolyte matrix and the underlying relaxation phenomena significantly influence ion transport in SPEs.[5,74,75] Specifically, in SPEs containing polyethylene oxide, it was well established that diffusivity correlates excellently with viscosity and polymer dynamics.[5,48,76,77] Similarly, viscosity and the ion-pair relaxation phenomena typically dictate the diffusivities in most liquid types of electrolytes. Since our pectin-loaded EC–LiTFSI electrolytes exhibit the features of both liquid and solid types of electrolytes, it will be crucial to understand the viscosity and relaxation phenomena. In particular, we want to ask the question: how are ionic diffusivities related to viscosity and various relaxation phenomena? In the following sections, we shed light on this question quantitatively by directly comparing the ionic diffusivity with the viscosity and the ion-pair structural relaxation timescales.

The viscosity calculations were carried out with the Green–Kubo formula[78–81] that uses the time correlation of the pressure tensor as:

$$\eta = \frac{V}{k_B T}\frac{1}{6}\sum_{\alpha\beta}\int_0^\infty \mathrm{d}\tau \langle P_{\alpha\beta}(t)P_{\alpha\beta}(t+\tau)\rangle \quad (4)$$

where $P_{\alpha\beta}$ is the pressure component, V is the volume, k_B is the Boltzmann constant and T is the absolute temperature. The ensemble average was taken over all 6 off-diagonal elements, $\alpha\beta = xy, xz, yz, yx, zx$, and zy, and 50 different trajectories were

generated from completely uncorrelated initial configurations. Since the pressure autocorrelation function is highly sensitive to the saving frequency, we recorded the trajectory of $P_{\alpha\beta}$ every 1 fs. The average of pressure autocorrelation functions along with the respective 50 independent runs, the corresponding running integrals, a detailed discussion on reducing numerical errors, and the extract of the Fortran code [full version of the code is available upon request] are shown in Fig. S5 and S6(b) in the ESI.†

The results of viscosity as a function of pectin wt% in EC–LiTFSI electrolytes are presented in Fig. 5(a). For neat EC–LiTFSI electrolytes, the viscosity was found to be 0.708 ± 0.200 mPa s at 425 K, off by a factor of ~3 compared to the experimental data.[82,83] A lower viscosity value compared to experiments is expected because the pair-wise interaction potential model does not capture the induced polarization effects completely, even if the scaled electrostatic interactions are employed in the potential model. We would like to mention that in MD simulations using pair-wise interactions, the calculated absolute values of the dynamical properties, such as the diffusion coefficient, conductivity and viscosity, are typically 5–10 times smaller than the experimental results.[82–84] Since the expected deviation is not significantly affected with the loading of pectin, there will be no change to different scaling relations considered in the paper such as $D \sim \tau_c^{\lambda}$ and $\eta \sim \tau_c^{\lambda}$. Therefore, since our focus is more towards understanding the scaling behavior such as $D \sim \tau_c^{\lambda}$ and $\eta \sim \tau_c^{\lambda}$, the absolute values of viscosity or diffusion coefficient are not critical. Furthermore, the viscosity changes slightly with pectin for lower loadings but rapidly for higher loadings beyond 5 wt%. At 50 wt%, the viscosity was calculated to be 170 ± 142 mPa s, about 250 times higher than that of neat EC–LiTFSI electrolytes. We note that our results of viscosity at a high wt% of pectin are somewhat erroneous due to high correlations in the autocorrelation function even with a trajectory of 10 ns containing pressure tensor components recorded at every 1 fs. Consequently, more statistics are required for higher wt%s to calculate the average viscosity and to understand the mechanical strength of the system. The analysis of viscosity correlations with the diffusion coefficient is presented in Fig. S7(a) and (b).†

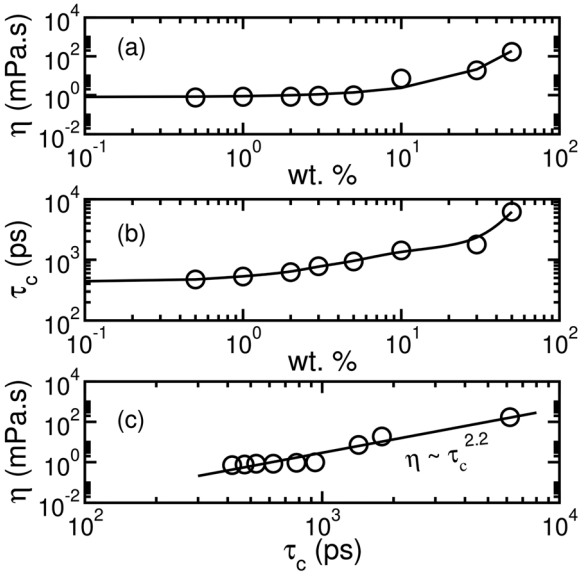

Fig. 5 (a) Viscosity and (b) ion-pair structural relaxation time (τ_c) as a function of pectin loading. (c) Viscosity values compared against the ion-pair relaxation timescale.

For the pectin–EC–LiTFSI system, different relaxation timescales may prevail in the system, such as polymer dynamics, hydrogen bond timescales, and ion-pair relaxation timescales. However, since our trajectories are only 300 ns long, estimating the relaxation phenomena associated with pectin polymer dynamics is not feasible. Moreover, the Li^+ and $TFSI^-$ ions are less prone to hydrogen bond formation in the EC electrolytes. Therefore, apart from the viscosity, we chose to analyze the ion-pair structural relaxation phenomena and examine their connection to the self-diffusion coefficients of ions.

To quantify the ion association relaxation phenomena, we computed the ion-pair correlation function $C(t)$, which signifies the relaxation behavior of all ion associations (see Fig. S8.1(a)†). The ion-pair correlation function $C(t)$ is defined as $C(t) = \frac{\langle h(t)h(0)\rangle}{\langle h(0)h(0)\rangle}$, where the angular bracket $\langle\cdots\rangle$ denotes an ensemble average over all ion-pairs and all possible time origins and $h(t)$ assigned a value unity if lithium and $TFSI^-$ ions are found within a specified cutoff distance, and zero otherwise. The cutoff distance defining the ion-pairs is chosen as 5 Å based on the extent of the first coordination shell of lithium and $TFSI^-$ ions. The ion motion correlates to the average ion association lifetimes, which quantifies the dynamics of breaking and the formation of the ion association. The ion-pair structural relaxation time was calculated using $\tau_c = \int_0^\infty a_0 \exp\left(-\left(\frac{t}{t^*}\right)^{\beta}\right)\mathrm{d}t = a_0 t^* \Gamma\left(1+\frac{1}{\beta}\right)$, where a_0, t^*, and β are the fitting parameters and Γ denotes the gamma function. The ion-pair relaxation time (τ_c) shows a similar qualitative trend with pectin loading (Fig. 5(b)), similar to that of viscosity. For a pure EC–LiTFSI electrolyte system, the ion-pair structural relaxation time was calculated to be 417 ps. With pectin loading, τ_c increases and reaches a maximum of 6185 ps for 50 wt% of pectin-loaded EC–LiTFSI electrolyte systems, an order of magnitude increase compared to the pristine EC–LiTFSI system. In addition to analyzing the cation–anion correlations, we also calculated the Li–EC and Li–pectin correlations to elucidate the interaction of Li ions with the solvent and polymer. The relaxation timescales associated with the atomic pairs between (a) Li and EC, (b) Li and TFSI, and (c) Li and pectin follow the trend: τ_c(Li–EC) < τ_c(Li–TFSI) ≪ τ_c(Li–pectin) and the corresponding numbers at a wt% of 10 are as follows: τ_c(Li–EC) = 78 ps, τ_c(Li–TFSI) = 1308 ps, and τ_c(Li–pectin) = 190 487 ps. Beyond this, we also calculated the effect of pectin on the lithium–pectin relaxation behavior and compared the same with Li–TFSI relaxation timescales. We found that the relaxation times of atomic pairs between (a) Li

and TFSI and (b) Li and pectin are related to the wt% of pectin in the following fashion: (a) $\tau_c^{\text{Li–TFSI}} = 503x^{0.49}$ and (b) $\tau_c^{\text{Li–pectin}} = 27\,815x^{0.85}$, where x is the wt% of pectin loading in EC–LiTFSI electrolytes (see Fig. S8.4†). We observed a strong correlation between the relaxation timescales of Li–pectin with the loading of pectin and a relatively moderate impact of pectin on the timescales of Li–TFSI pairs. This observation suggests that the lithium ion interacts with the polymer strongly, which helps in ion-pair dissociation, promoting smaller ionic clusters. The above findings reveal that pectin can be a good option for battery applications for proving good ionic conductivity, biodegradability, and mechanical stability.

Our analysis of η and τ_c concluded that while η increases by a factor of 250 for the highest pectin loading studied in this work, τ_c increases only by a factor of 15. Therefore, the rate of increase of the viscosity and ion-pair structural relaxation time with pectin loading follows different trends, implying that either both or none of these quantities may explain the ionic diffusivities in the electrolytes according to the Stokes–Einstein formula, $D = k_BT/6\pi\eta R$, where R is the hydrodynamic radius of the spherical particle suspended in a model fluid. To establish more clearly the relationship between the viscosity and ion-pair structural relaxation timescales, we analyzed the correlation between the viscosity and the ion-pair correlation timescales through $\eta \sim \tau_c^{\lambda}$ as shown in Fig. 5(c) and obtained the exponent, $\lambda = 2.2$, which does not show a one-to-one correlation between η and τ_c. The above result establishes a rapid change in viscosity with the structural relaxation time. As we do not observe a one-to-one correlation between the viscosity and the ion-pair structural relaxation time, we examined the effect of both the viscosity and ion-pair structural relaxation timescales on the diffusivity of ionic species.

In Fig. 6(a) and (b), we displayed the diffusivity of ions against the ion-pair relaxation timescales for the Li^+ and $TFSI^-$ ions, respectively. For the Li^+ and $TFSI^-$ ions, the diffusivity decreases quite distinctly with the ion-pair relaxation timescales. Specifically, for the $TFSI^-$ ions, by fitting diffusivities to the respective power laws, $D_+ \sim \tau_c^{-\lambda}$ and $D_- \sim \tau_c^{-\lambda}$, we obtained the exponents of 3.1 and 0.95, respectively. Clearly, we do not observe direct correlations between the diffusivity of Li^+ ions and the ion-pair relaxation timescales (*i.e.*, $D_+ \sim \tau_c^{-3.1}$). The excellent correlations found between the diffusivity of $TFSI^-$ ions and ion-pair relaxation timescales (*i.e.*, $D_- \sim \tau_c^{-0.95}$) are similar to those reported for traditional liquid electrolytes.[49,74,85,86]

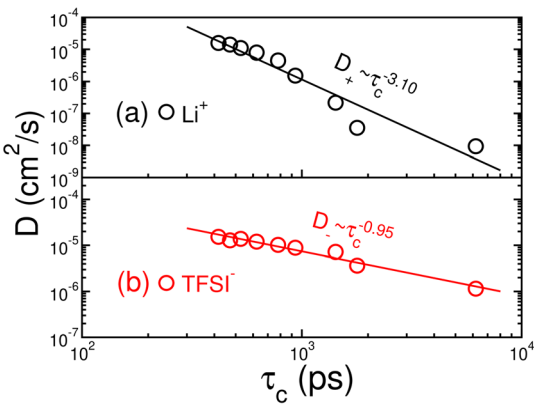

Fig. 6 Correlations between (a) the diffusion coefficient of Li^+ ions and ion-pair relaxation timescales and (b) the diffusion coefficient of $TFSI^-$ ions and ion-pair relaxation timescales.

The above analysis establishes that the Li^+ ions are transported in the electrolyte through distinct transport mechanisms other than the underlying ion-pair structural relaxation phenomena. Since the lithium ions are strongly coordinated with the pectin chains, as noted from the respective $g(r)$, CN(r), and $P(n)$ plots (see Fig. S2†), we propose that the pectin chains facilitate lithium ion transport along the backbone on longer timescales (likely microseconds and even longer), similar to those reported for other electrolytes containing synthetic polymers.[32,74,76,86,87] However, a further thorough analysis of long time Li^+ ion transport along the pectin backbone and analysis of the respective relaxation timescales are required to establish such a hypothesis. We refrain from such an ambitious task because of the relatively short trajectories (300 ns for wt% of up to 5 and 500 ns for higher loading systems) we could generate in this work. Since $D_+ \sim \tau_c^{-3.1}$ is also a clear indication of decoupling between the ion transport properties and the structural relaxations, there is a huge scope to achieve the twin goal of the highest ionic conductivity and mechanical stability in a single battery electrolyte.[32,74,85]

The above analysis and the results in Fig. 6 point to a characteristic behavior of pectin–EC–LiTFSI electrolytes that either obey or disobey the diffusivity power-law relation $D \sim \tau_c^{-1}$ for a given type of ionic species. To the best of our knowledge, no soft matter or battery electrolyte material exhibits this unique feature, offering the flexibility of designing a new class of electrolytes for optimizing either cation or anion conductivity and mechanical strength. Explicitly, the validity of diffusivity power-law relationship $D \sim \tau_c^{-1}$ inherently indicates the ability of experimental design strategies to increase the ionic conductivity of the electrolyte at the expense of its mechanical strength. The $D \sim \tau_c^{-1}$ relationship is commonly observed to be obeyed in a majority of liquid electrolytes and ionic liquid electrolytes, in which τ_c can be controllably tuned to attain high ionic conductivity.[76,88] On the other hand, the breakdown of diffusivity power-law relationship $D \sim \tau_c^{-1}$ offers interesting consequences that both the ionic conductivity and the mechanical strength of the electrolyte can be optimized simultaneously.[49,74,89] Since $TFSI^-$ ions obey the diffusivity power-law relationship (*i.e.*, $D_- \sim \tau_c^{-0.95}$) in pectin–EC–LiTFSI electrolytes, τ_c can be tuned to increase the ionic diffusivity/conductivity, for example, by adding plasticizers to pectin–EC–LiTFSI electrolytes. On the other hand, since Li^+ ions disobey the diffusivity power-law relationship (*i.e.*, $D_+ \sim \tau_c^{-3.1}$), the mechanical strength of the electrolyte can be tuned, which does not affect the Li^+ ion diffusivity. Therefore, both the validity and breakdown of $D \sim \tau_c^{-1}$ offers flexibility in simultaneously increasing the ionic conductivity and viscosity/

mechanical strength[32,74,85] with a huge promise to experimental approaches in synthesizing novel pectin–EC–LiTFSI electrolytes. In this context, however, further investigations (both simulations and experiments) are required to understand the effect of plasticizers on the ion transport mechanisms in pectin–EC–LiTFSI electrolytes.

Now, the question is, what can we expect from this relative variation of diffusivity on ionic conductivity for different ions? As the ionic diffusivity of Li^+ ions is ~100 times less than that of $TFSI^-$ ions, we can expect a negligible contribution towards ionic conductivity arising from Li^+ ions for higher wt%s of pectin chains. Therefore, our designed electrolytes might behave as single-ion conductors. We will expand on this phenomenon in the following sections.

Ionic conductivity of pectin–EC–LiTFSI electrolytes

The most crucial parameter in determining the suitability of an electrolyte for rechargeable batteries is its ability to conduct ionic charges efficiently between the electrodes. Electrolytes offering the least resistance to the conduction of ions are highly desired for the design of rechargeable batteries. Designing a battery electrolyte with superior ionic conductivity and high viscosity simultaneously is the holy grail of solid polymer electrolyte research. The Nernst–Einstein (NE) equation $\sigma_{NE} = \frac{e^2}{Vk_BT}\left(N_{Li}z_{Li}^2\tilde{D}_{Li} + N_{TFSI}z_{TFSI}^2\tilde{D}_{TFSI}\right)$ [70,90] for ionic conductivity can give excellent results for dilute solutions because of the highly uncorrelated motion of ions; in the NE equation, e is the electronic charge, V is the volume, k_B is the Boltzmann constant, and T is the absolute temperature. The symbols N_α, Z_α, D_α, and α = Li, TFSI indicate the number, ionic charge, and diffusion coefficients of Li^+ ions and $TFSI^-$ ions, respectively. However, the NE equation provides only an upper limit for the ionic conductivity at higher salt concentrations since the ion–ion correlations start to dominate to lower the ionic conductivity. For instance, Borodin *et al.*[91] reported that about 20–30% of the total ionic conductivity were reduced because of the correlated motion of ions at a relatively high salt concentration of EC : Li ratios of 20 : 1 and 10 : 1. Similarly, in a different electrolyte system (PEO–LiTFSI) at an intermediate level of the salt concentration measured in terms of EO : Li ratios of 39 : 1 and 20 : 1, about 5–10% of the correlations were reported.[50] Since the concentration of LiTFSI salt is considerably low (EC : Li = 48 : 1) in all of our systems compared to the literature,[5] the cation–anion correlations will not be significant. Therefore, the NE relationship can serve as a decent option for understanding the qualitative behavior of the ionic conductivity of pectin–EC–LiTFSI electrolytes.[70]

As shown in Fig. 7, the Nernst–Einstein conductivity of pure EC is 0.0123 S cm^{-1}, which agrees well with the experimental ionic conductivity[92] and previous calculations based on MD simulations.[91] From our calculations, we observed a decrease in ionic conductivity similar to ionic diffusivity with the loading of pectin. The lowering of ionic conductivity with the addition of pectin is a direct consequence of the stronger interaction of lithium ions with the electronegative charge groups abundant in pectin chains. When the EC–LiTFSI system is loaded with 10 wt% of pectin, the ionic conductivity decreases by a factor of four. Despite the ionic conductivity being lower in higher wt%s of pectin, we expect that the ionic correlations to be insignificant, as clearly suggested by $P(n)$ that the formation of smaller ionic clusters over the larger ones is more probable at high loadings of pectin. Therefore, owing to the trade-off between the decrease in σ_{NE} and the decrease in ionic aggregates, the 'true' or 'full' ionic conductivity (*i.e.*, ionic conductivity that includes effects arising from ion–ion correlations, unlike σ_{NE} which does not include contributions due to ion–ion correlations) will have fewer detrimental effects contributed by the correlated motion of ions at optimal loadings of pectin.

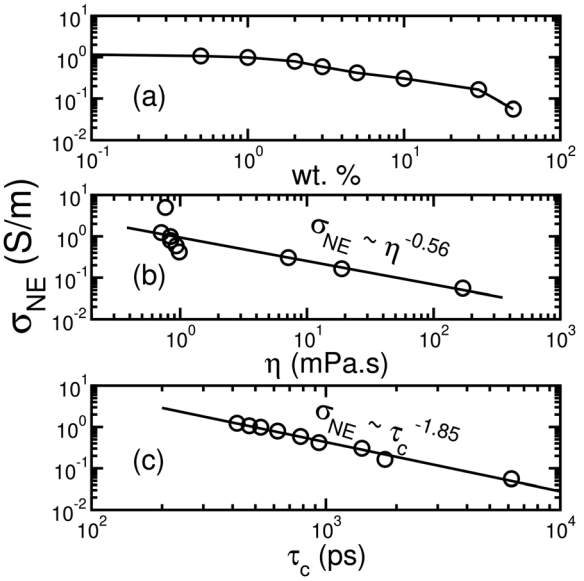

Fig. 7 Nernst–Einstein ionic conductivity as a function of the (a) wt% of pectin loading, (b) viscosity, and (c) ion-pair relaxation time.

For the experimental design and technological development of viable pectin–EC–LiTFSI electrolytes, smaller loadings of pectin cannot offer better mechanical strength (due to the low increase in η), even though the ionic conductivity is not significantly affected. On the other hand, high loadings of pectin beyond 20 wt% lack the required ionic conductivity for battery applications, and therefore, is not recommended for the experimental design despite offering high mechanical strength. Based on the observed overall trends for the rate of change of σ_{NE}, η, $P(0)$, $P(1)$ and $P(2)$ with the loading of pectin and an intuitive objective function, $f(\sigma_{NE}, P(0), P(1)) \sim \sigma_{NE}P^a(0)/P^b(1)$ (see Fig. S9†), we propose that pectin–EC–LiTFSI electrolytes offer efficient ionic conductivity and optimal mechanical strength at intermediate loadings of pectin in the range of 10–15 wt%s. However, further analysis of different types of ionic aggregates containing at least 2 cations and at least 2 anions simultaneously and their effect on ionic conductivity is required to fully understand the 'true' ionic conductivity.[70] Furthermore, since the rate of decrease of the

diffusion coefficient of Li^+ ions is higher than that of $TFSI^-$ ions, the $TFSI^-$ ions contribute largely to the total ionic conductivity of the pectin-loaded EC–LITFSI systems. Our systems may be considered excellent ion conductors if we can increase the ionic conductivity of cations. Future research can focus on increasing the ion conductivity of cations by increasing the transference of cations through the electrolytes (see Fig. S10†). The outcomes of this work have provided an idea of how pectin influences the transport mechanisms of EC–LiTFSI electrolytes. It is, therefore, possible to design experimental strategies to improve the pectin-based electrolyte conductivity and transference numbers. We recommend designing electrolytes with lower pectin loading (10–15 wt%, based on the intuitive objective function) using a different liquid electrolyte instead of EC and incorporating additives to enhance the ionic conductivity without compromising their mechanical stability. In fact, in our recent work,[93] we have shown that the transference numbers are more than 0.55 in pectin–ionic liquid electrolytes. Another strategy is to tune the salt concentration to improve the conductivity for the proposed optimal choice of 10–15 wt% of pectin loading.

Similar to the mechanisms examined for ionic diffusivity, we analyzed the correlations between NE conductivity and viscosity/ion-pair relaxations and found that the viscosity and ion-pair relaxation timescales highly influence the Nernst–Einstein conductivity. Interestingly, we found significant differences between σ_{NE} *vs.* η^{λ} and σ_{NE} *vs.* ${\tau_c}^{\lambda}$ as shown in Fig. 7 (b and c). Explicitly, we observed that the NE conductivity depends on viscosity as $\sigma_{NE} \sim \eta^{-0.56}$ while on the ion-pair relaxation timescales as $\sigma_{NE} \sim {\tau_c}^{-1.85}$, implying that (i) there exists distinct transport mechanisms for ionic conductivity and (ii) that neither of η and τ_c correlates to NE conductivity. Despite the lower correlated motion of ions prevailing at a low salt concentration of EC : Li = 48 : 1, the above results suggest that the respective ion-pair relaxation times influence the ionic conductivity and that the existence of smaller ionic clusters can still negatively impact the ionic conductivity.

Before concluding, we want to emphasize that we proposed pectin for battery electrolyte applications in EC–LITFSI liquid electrolytes for the first time using simulations. Therefore, to date, there is no experimental literature on pectin–EC–LiTFSI electrolytes to compare our simulations with, to the best of our knowledge.[93] Despite that, we conducted a brief comparison of the pectin–EC–LiTFSI [biopolymer] electrolytes simulated in this work with conventional [synthetic] polymer electrolytes such as PEO–LiTFSI electrolytes (see Table 2).

Table 2 Comparison of some important physical parameters obtained in this work with the literature

Quantity	Pectin–EC–LiTFSI at 10 wt% (this work, 425 K)	PEO–LiTFSI (literature)
ρ (kg m^{-3})	1230	1129 at 353 K [9]
$CN_{Li-TFSI}$	0.214	0.5 [5]
$CN_{Li-O(polymer)}$	1.478	3.85 [5]
D^+ (cm^2 s^{-1})	2.17×10^{-7}	3×10^{-7} at 400 K [94] 4.7×10^{-7} at 400 K [95]
D^- (cm^2 s^{-1})	7.21×10^{-7}	8×10^{-7} at 400 K [94] 10.8×10^{-7} at 400 K [95]
σ (S cm^{-1})	3.8×10^{-3}	5.5×10^{-3} at 373 K [96] 4.0×10^{-3} at 393 K [97]

Conclusions

In summary, we simulated a new class of solid polymer electrolytes derived from the biopolymer pectin chains that have enormous potential to convert the traditional liquid EC–LiTFSI electrolytes into solid polymer electrolytes and are environmentally compatible.

Our simulations predict that pectin has excellent ion solvating capabilities, as good as those of EC and polyethylene oxide chains, because of its structural uniqueness. We studied its structural properties by calculating the radial distribution function, coordination number, and different types of association probabilities. We found that the addition of pectin chains increases the number of free lithium ions (*i.e.*, lithium ions that are free from their coordination with $TFSI^-$ counterions) in the first coordination shell due to the enhanced coordination with the electronegative groups of the pectin polymer chain. Furthermore, our simulations show an increase in the probability of association of polymer units around the lithium ions, resulting in reduced Li^+ ion coordination with counterions and stronger lithium–pectin interactions. As a result, the pectin promotes smaller ionic aggregates over larger ionic aggregates, in contrast to those typically reported in liquid and polymer electrolytes. The formation of smaller ionic aggregates over larger ionic aggregates is a promising feature of pectin and an interesting outcome for future battery electrolyte designs, favoring the uncorrelated motion of ionic species and, thereby, efficient ionic conductivity.

The overall ion diffusivity follows a decreasing trend with the loading of pectin chains due to the strong coordination between Li^+ ions and polymer chains. However, the diffusion of both the ions at low pectin loadings (up to 3 wt%) is almost unaffected by pectin and decreases by a factor of 100 for the lithium ion at higher loadings. A similar output is observed for the Nernst–Einstein conductivity due to the lower diffusion of Li^+ ions. As expected, from the transference number calculations, we observed that the ionic conductivity depends heavily on the $TFSI^-$ ions and the contribution of Li^+ ions towards conductivity is insignificant.

By comparing the diffusivity of ions and ion-pair relaxation timescales, we found interesting trends for the $D \sim {\tau_c}^{-\lambda}$ relationship. Explicitly, while the diffusivity of $TFSI^-$ ions obeys the $D_- \sim {\tau_c}^{-1}$ relationship with ion-pair relaxation timescales (*i.e.*, $TFSI^-$ ions follow $D_- \sim {\tau_c}^{-0.95}$), the diffusivity of Li^+ ions does not obey the $D_+ \sim {\tau_c}^{-1}$ relationship (*i.e.*, Li^+ ions follow $D_+ \sim {\tau_c}^{-3.1}$). The excellent correlations found between the diffusivity of $TFSI^-$ ions and ion-pair relaxation timescales are consistent with previous reports.[49,74,85,86] The lithium ion diffusivity does not correlate with the ion-pair relaxation time

because the polymeric pectin units trap the lithium ions. The Nernst–Einstein conductivity scales with ion-pair relaxation timescales as $\sigma_{NE} \sim \tau_c^{-1.85}$, revealing distinct transport mechanisms for ionic conductivity.

Our simulations established a surprising feature unique to the pectin–EC–LiTFSI electrolytes: both the validity and violation of the $D \sim \tau_c^{-1}$ relationship for a given type of ionic species for the dependency of diffusion coefficient with τ_c. To the best of our knowledge, no soft matter or battery electrolyte material exhibits such a unique feature, offering the flexibility of designing a new class of electrolytes for optimizing cation or anion conductivity. The reduced ion clustering, higher mechanical strength, and biodegradability are the futuristic advantages of the biopolymer pectin that make it a promising alternative material to the existing state-of-the-art electrolyte technologies.

Conflicts of interest

The authors have no conflicts to disclose.

Acknowledgements

We thank Ananya Debnath for insightful discussions and critical feedback on the manuscript. The authors acknowledge the Computer Center of IIT Jodhpur and the HPC center at the Department of Physics, Freie Universität Berlin (**https://doi.org/10.17169/refubium-26754**) for providing computing resources that have contributed to the research results reported in this paper. RRN acknowledges the support by Deutsche Forschungsgemeinschaft, Grant No. CRC 1349, Code No. 387284271, Project No. C04. SM acknowledges the support from the Science and Engineerign Research Board (SERB) International Research Experience Fellowship SIR/2022/000786 and CRG/2019/000106 provided by the Department of Science and Technology (DST), India. PKJ acknowledges support from IIT Jodhpur through the Seed Grant (I/SEED/PKJ/20220016) and the DST through a SERB-CRG Grant No. CRG/2022/006365.

References

1 Z. Xue, D. He and X. Xie, Poly(Ethylene Oxide)-Based Electrolytes for Lithium-Ion Batteries, *J. Mater. Chem. A*, 2015, 19218–19253, DOI: **10.1039/c5ta03471j**.

2 J. B. Goodenough and K. S. Park, The Li-Ion Rechargeable Battery: A Perspective, *J. Am. Chem. Soc.*, 2013, 1167–1176, DOI: **10.1021/ja3091438**.

3 T. Winie, A. K. Arof and S. Thomas, *Polymer Electrolytes: Characterization Techniques and Energy Applications*, John Wiley & Sons, 2019.

4 M. Armand, P. Bruce, M. Forsyth, B. Scrosati and W. Wieczorek, Polymer Electrolytes, *Energy Materials*, 2011, ch. 1, pp. 1–31. DOI: **10.1002/9780470977798.ch1**.

5 O. Borodin and G. D. Smith, Mechanism of Ion Transport in Amorphous Poly(Ethylene Oxide)/LiTFSI from Molecular Dynamics Simulations, *Macromolecules*, 2006, **39**(4), 1620–1629, DOI: **10.1021/ma052277v**.

6 A. Manthiram, X. Yu and S. Wang, Lithium Battery Chemistries Enabled by Solid-State Electrolytes, *Nat. Rev. Mater.*, 2017, **2**(4), 1–16, DOI: **10.1038/natrevmats.2016.103**.

7 S. Xia, X. Wu, Z. Zhang, Y. Cui and W. Liu, Practical Challenges and Future Perspectives of All-Solid-State Lithium-Metal Batteries, *Chem*, 2019, **5**(4), 753–785, DOI: **10.1016/j.chempr.2018.11.013**.

8 R. Singh, A. R. Polu, B. Bhattacharya, H. W. Rhee, C. Varlikli and P. K. Singh, Perspectives for Solid Biopolymer Electrolytes in Dye Sensitized Solar Cell and Battery Application, *Renewable Sustainable Energy Rev.*, 2016, 1098–1117, DOI: **10.1016/j.rser.2016.06.026**.

9 N. Molinari, J. P. Mailoa and B. Kozinsky, Effect of Salt Concentration on Ion Clustering and Transport in Polymer Solid Electrolytes: A Molecular Dynamics Study of PEO–LiTFSI, *Chem. Mater.*, 2018, **30**(18), 6298–6306, DOI: **10.1021/acs.chemmater.8b01955**.

10 Y. Li, B. Xu, H. Xu, H. Duan, X. Lü, S. Xin, W. Zhou, L. Xue, G. Fu, A. Manthiram and J. B. Goodenough, Hybrid Polymer/Garnet Electrolyte with a Small Interfacial Resistance for Lithium-Ion Batteries, *Angew. Chem., Int. Ed.*, 2017, **56**(3), 753–756, DOI: **10.1002/ANIE.201608924**.

11 Q. Zhou, J. Ma, S. Dong, X. Li and G. Cui, Intermolecular Chemistry in Solid Polymer Electrolytes for High-Energy-Density Lithium Batteries, *Adv. Mater.*, 2019, **31**(50), 1902029, DOI: **10.1002/adma.201902029**.

12 Z. Lv, Q. Zhou, S. Zhang, S. Dong, Q. Wang, L. Huang, K. Chen and G. Cui, Cyano-Reinforced in-Situ Polymer Electrolyte Enabling Long-Life Cycling for High-Voltage Lithium Metal Batteries, *Energy Storage Mater.*, 2021, **37**, 215–223, DOI: **10.1016/j.ensm.2021.01.017**.

13 Q. Zhou, S. Dong, Z. Lv, G. Xu, L. Huang, Q. Wang, Z. Cui and G. Cui, A Temperature-Responsive Electrolyte Endowing Superior Safety Characteristic of Lithium Metal Batteries, *Adv. Energy Mater.*, 2020, **10**(6), 1903441, DOI: **10.1002/aenm.201903441**.

14 H. Duan, F. Oluwatemitope, S. Wu, H. Zheng, Y. Zou, G. Li, Y. Wu and H. Liu, Li/Garnet Interface Optimization: An Overview, *ACS Appl. Mater. Interfaces*, 2020, **12**(47), 52271–52284, DOI: **10.1021/acsami.0c16966**.

15 N. Riphaus, B. Stiaszny, H. Beyer, S. Indris, H. A. Gasteiger and S. J. Sedlmaier, Understanding Chemical Stability Issues between Different Solid Electrolytes in All-Solid-State Batteries, *J. Electrochem. Soc.*, 2019, **166**(6), A975–A983, DOI: **10.1149/2.0351906jes**.

16 N. Molinari, J. P. Mailoa and B. Kozinsky, Effect of Salt Concentration on Ion Clustering and Transport in Polymer Solid Electrolytes: A Molecular Dynamics Study of PEO-LiTFSI, *Chem. Mater.*, 2018, **30**(18), 6298–6306, DOI: **10.1021/acs.chemmater.8b01955**.

17 X. Jia, Y. Yang, C. Wang, C. Zhao, R. Vijayaraghavan, D. R. Macfarlane, M. Forsyth and G. G. Wallace,

Biocompatible Ionic Liquid-Biopolymer Electrolyte-Enabled Thin and Compact Magnesium-Air Batteries, *ACS Appl. Mater. Interfaces*, 2014, **6**(23), 21110–21117, DOI: 10.1021/am505985z.

18 L. S. Ng and A. A. Mohamad, Protonic Battery Based on a Plasticized Chitosan-NH_4NO_3 Solid Polymer Electrolyte, *J. Power Sources*, 2006, **163**(1 SPEC. ISS.), 382–385, DOI: 10.1016/j.jpowsour.2006.09.042.

19 S. Y. Xiao, Y. Q. Yang, M. X. Li, F. X. Wang, Z. Chang, Y. P. Wu and X. Liu, A Composite Membrane Based on a Biocompatible Cellulose as a Host of Gel Polymer Electrolyte for Lithium Ion Batteries, *J. Power Sources*, 2014, **270**, 53–58, DOI: 10.1016/J.JPOWSOUR.2014.07.058.

20 M. Doi, *Soft Matter Physics*, Oxford University Press, United Kingdom, 1st edn, 2013.

21 P. Nelson, *Biological Physics: Energy, Information, Life*, W. H. Freeman & Co. Ltd, 2003.

22 R. Singh, A. R. Polu, B. Bhattacharya, H. W. Rhee, C. Varlikli and P. K. Singh, Perspectives for Solid Biopolymer Electrolytes in Dye Sensitized Solar Cell and Battery Application, *Renewable Sustainable Energy Rev.*, 2016, 1098–1117, DOI: 10.1016/j.rser.2016.06.026.

23 M. Rayung, M. M. Aung, S. C. Azhar, L. C. Abdullah, M. S. Su'ait, A. Ahmad and S. N. A. M. Jamil, Bio-Based Polymer Electrolytes for Electrochemical Devices: Insight into the Ionic Conductivity Performance, *Materials*, 2020, **13**(4), 838, DOI: 10.3390/ma13040838.

24 B. Manunza, S. Deiana and C. Gessa, Molecular Dynamics of Pectic Substances, *Theoretical and Computational Chemistry*, Elsevier, 1999, ch. 22, vol. 7, pp. 899–932. DOI: 10.1016/S1380-7323(99)80055-7.

25 J. Gou, W. Liu and A. Tang, A Renewable Gel Polymer Electrolyte Based on the Different Sized Carboxylated Cellulose with Satisfactory Comprehensive Performance for Rechargeable Lithium Ion Battery, *Polymer*, 2020, **208**, 122943, DOI: 10.1016/J.POLYMER.2020.122943.

26 Y. Lin, Y. Cheng, J. Li, J. D. Miller, J. Liu and X. Wang, Biocompatible and Biodegradable Solid Polymer Electrolytes for High Voltage and High Temperature Lithium Batteries, *RSC Adv.*, 2017, **7**(40), 24856–24863, DOI: 10.1039/C7RA01601H.

27 B. Zhou, D. He, J. Hu, Y. Ye, H. Peng, X. Zhou, X. Xie and Z. Xue, A Flexible, Self-Healing and Highly Stretchable Polymer Electrolyte *via* Quadruple Hydrogen Bonding for Lithium-Ion Batteries, *J. Mater. Chem. A*, 2018, **6**(25), 11725–11733, DOI: 10.1039/C8TA01907J.

28 E. Lizundia, D. Kundu, E. Lizundia and D. Kundu, Advances in Natural Biopolymer-Based Electrolytes and Separators for Battery Applications, *Adv. Funct. Mater.*, 2021, **31**(3), 2005646, DOI: 10.1002/ADFM.202005646.

29 K.-H. Shen and L. M. Hall, Effects of Ion Size and Dielectric Constant on Ion Transport and Transference Number in Polymer Electrolytes, *Macromolecules*, 2020, **53**(22), 10086–10096, DOI: 10.1021/acs.macromol.0c02161.

30 J. J. Hu, G. K. Long, S. Liu, G. R. Li and X. P. Gao, A LiFSI–LiTFSI Binary-Salt Electrolyte to Achieve High Capacity and Cycle Stability for a Li–S Battery, *Chem. Commun.*, 2014, **50**(93), 14647–14650, DOI: 10.1039/C4CC06666A.

31 J. N. BeMiller, *An Introduction to Pectins: Structure and Properties*, 1986, pp. 2–12. DOI: 10.1021/bk-1986-0310.ch001.

32 S. Mogurampelly and V. Ganesan, Structure and Mechanisms Underlying Ion Transport in Ternary Polymer Electrolytes Containing Ionic Liquids, *J. Chem. Phys.*, 2017, **146**(7), 074902, DOI: 10.1063/1.4976131.

33 R. Bouchet, S. Maria, R. Meziane, A. Aboulaich, L. Lienafa, J. P. Bonnet, T. N. T. Phan, D. Bertin, D. Gigmes, D. Devaux, R. Denoyel and M. Armand, Single-Ion BAB Triblock Copolymers as Highly Efficient Electrolytes for Lithium-Metal Batteries, *Nat. Mater.*, 2013, **12**(5), 452–457, DOI: 10.1038/nmat3602.

34 A. G. Moreira and R. R. Netz, Strong-Coupling Theory for Counter-Ion Distributions, *Europhys. Lett.*, 2000, **52**(6), 705–711, DOI: 10.1209/epl/i2000-00495-1.

35 A. Naji, S. Jungblut, A. G. Moreira and R. R. Netz, Electrostatic Interactions in Strongly Coupled Soft Matter, *Phys. A*, 2005, **352**(1), 131–170, DOI: 10.1016/j.physa.2004.12.029.

36 S. Fischer, A. Naji and R. R. Netz, Salt-Induced Counterion-Mobility Anomaly in Polyelectrolyte Electrophoresis, *Phys. Rev. Lett.*, 2008, **101**(17), 176103, DOI: 10.1103/PhysRevLett.101.176103.

37 J. R. Andrade, E. Raphael and A. Pawlicka, Plasticized Pectin-Based Gel Electrolytes, *Electrochim. Acta*, 2009, **54**(26), 6479–6483, DOI: 10.1016/j.electacta.2009.05.098.

38 P. Perumal, P. Christopher Selvin, S. Selvasekarapandian and K. P. Abhilash, Bio-Host Pectin Complexed with Dilithium Borate Based Solid Electrolytes for Polymer Batteries, *Mater. Res. Express*, 2019, **6**(11), 115513, DOI: 10.1088/2053-1591/ab4724.

39 H. J. C. Berendsen, D. Van Der Spoel and R. Van Drunen, *GROMACS: A Message-Passing Parallel Molecular Dynamics Implementation PROGRAM SUMMARY Title of Program, GROMACS Version 1.0*, 1995, vol. 91.

40 D. Van Der Spoel, E. Lindahl, B. Hess, G. Groenhof, A. E. Mark and H. J. C. Berendsen, GROMACS: Fast, Flexible, and Free, *J. Comput. Chem.*, 2005, **26**(16), 1701–1718, DOI: 10.1002/JCC.20291.

41 U. Essmann, L. Perera, M. L. Berkowitz, T. Darden, H. Lee and L. G. Pedersen, A Smooth Particle Mesh Ewald Method, *J. Chem. Phys.*, 1998, **103**(19), 8577, DOI: 10.1063/1.470117.

42 W. L. Jorgensen, D. S. Maxwell and J. Tirado-Rives, Development and Testing of the OPLS All-Atom Force Field on Conformational Energetics and Properties of Organic Liquids, *J. Am. Chem. Soc.*, 1996, **118**(45), 11225–11236, DOI: 10.1021/ja9621760.

43 B. Doherty, X. Zhong, S. Gathiaka, B. Li and O. Acevedo, Revisiting OPLS Force Field Parameters for Ionic Liquid Simulations, *J. Chem. Theory Comput.*, 2017, **13**(12), 6131–6135, DOI: 10.1021/ACS.JCTC.7B00520.

44 B. J. Kirby and P. Jungwirth, Charge Scaling Manifesto: A Way of Reconciling the Inherently Macroscopic and

Microscopic Natures of Molecular Simulations, *J. Phys. Chem. Lett.*, 2019, **10**(23), 7531–7536, DOI: 10.1021/ACS.JPCLETT.9B02652.

45 V. V. Chaban, I. V. Voroshylova and O. N. Kalugin, A New Force Field Model for the Simulation of Transport Properties of Imidazolium-Based Ionic Liquids, *Phys. Chem. Chem. Phys.*, 2011, **13**(17), 7910–7920, DOI: 10.1039/C0CP02778B.

46 V. Chaban, Polarizability versus Mobility: Atomistic Force Field for Ionic Liquids, *Phys. Chem. Chem. Phys.*, 2011, **13**(35), 16055–16062, DOI: 10.1039/C1CP21379B.

47 I. Leontyev and A. Stuchebrukhov, Accounting for Electronic Polarization in Non-Polarizable Force Fields, *Phys. Chem. Chem. Phys.*, 2011, **13**(7), 2613–2626, DOI: 10.1039/C0CP01971B.

48 S. Mohapatra, S. Sharma, A. Sriperumbuduru, S. R. Varanasi and S. Mogurampelly, Effect of Succinonitrile on Ion Transport in PEO-Based Lithium-Ion Battery Electrolytes, *J. Chem. Phys.*, 2022, **156**(21), 214903, DOI: 10.1063/5.0087824.

49 S. Mogurampelly, J. R. Keith and V. Ganesan, Mechanisms Underlying Ion Transport in Polymerized Ionic Liquids, *J. Am. Chem. Soc.*, 2017, **139**(28), 9511–9514, DOI: 10.1021/JACS.7B05579.

50 O. Borodin and G. D. Smith, LiTFSI Structure and Transport in Ethylene Carbonate from Molecular Dynamics Simulations, *J. Phys. Chem. B*, 2006, **110**(10), 4971–4977, DOI: 10.1021/JP056249Q.

51 K. N. Kirschner, A. B. Yongye, S. M. Tschampel, J. González-Outeiriño, C. R. Daniels, B. L. Foley and R. J. Woods, GLYCAM06: A Generalizable Biomolecular Force Field. Carbohydrates, *J. Comput. Chem.*, 2008, **29**(4), 622–655, DOI: 10.1002/jcc.20820.

52 A. D. McLean and G. S. Chandler, Contracted Gaussian Basis Sets for Molecular Calculations. I. Second Row Atoms, Z = 11–18, *J. Chem. Phys.*, 1980, **72**(10), 5639–5648, DOI: 10.1063/1.438980.

53 R. Krishnan, J. S. Binkley, R. Seeger and J. A. Pople, Self-consistent Molecular Orbital Methods. XX. A Basis Set for Correlated Wave Functions, *J. Chem. Phys.*, 1980, **72**(1), 650–654, DOI: 10.1063/1.438955.

54 M. J. Frisch, G. W. Trucks, H. B. Schlegel, G. E. Scuseria, M. A. Robb, J. R. Cheeseman, G. Scalmani, V. Barone, G. A. Petersson, H. Nakatsuji, X. Li, M. Caricato, A. V. Marenich, J. Bloino, B. G. Janesko, R. Gomperts, B. Mennucci, H. P. Hratchian, J. V. Ortiz, A. F. Izmaylov, J. L. Sonnenberg, D. Williams-Young, F. Ding, F. Lipparini, F. Egidi, J. Goings, B. Peng, A. Petrone, T. Henderson, D. Ranasinghe, V. G. Zakrzewski, J. Gao, N. Rega, G. Zheng, W. Liang, M. Hada, M. Ehara, K. Toyota, R. Fukuda, J. Hasegawa, M. Ishida, T. Nakajima, Y. Honda, O. Kitao, H. Nakai, T. Vreven, K. Throssell, J. A. Montgomery Jr., J. E. Peralta, F. Ogliaro, M. J. Bearpark, J. J. Heyd, E. N. Brothers, K. N. Kudin, V. N. Staroverov, T. A. Keith, R. Kobayashi, J. Normand, K. Raghavachari, A. P. Rendell, J. C. Burant, S. S. Iyengar, J. Tomasi, M. Cossi, J. M. Millam, M. Klene, C. Adamo, R. Cammi, J. W. Ochterski, R. L. Martin, K. Morokuma, O. Farkas, J. B. Foresman and D. J. Fox, *Gaussian 16, Revision C.01*, 2016.

55 H. B. Schlegel, Optimization of Equilibrium Geometries and Transition Structures, *J. Comput. Chem.*, 1982, **3**(2), 214–218, DOI: 10.1002/JCC.540030212.

56 C. I. Bayly, P. Cieplak, W. Cornell and P. A. Kollman, A Well-Behaved Electrostatic Potential Based Method Using Charge Restraints for Deriving Atomic Charges: The RESP Model, *J. Phys. Chem.*, 1993, **97**(40), 10269–10280, DOI: 10.1021/j100142a004.

57 D. Mohnen, Pectin Structure and Biosynthesis, *Curr. Opin. Plant Biol.*, 2008, **11**(3), 266–277, DOI: 10.1016/J.PBI.2008.03.006.

58 L. Martinez, R. Andrade, E. G. Birgin and J. M. Martínez, PACKMOL: A Package for Building Initial Configurations for Molecular Dynamics Simulations, *J. Comput. Chem.*, 2009, **30**(13), 2157–2164, DOI: 10.1002/JCC.21224.

59 V. Nilsson, A. Kotronia, M. Lacey, K. Edström and P. Johansson, Highly Concentrated LiTFSI-EC Electrolytes for Lithium Metal Batteries, *ACS Appl. Energy Mater.*, 2020, **3**(1), 200–207, DOI: 10.1021/ACSAEM.9B01203.

60 M. Bolloli, F. Alloin, J. Kalhoff, D. Bresser, S. Passerini, P. Judeinstein, J. C. Leprêtre and J. Y. Sanchez, Effect of Carbonates Fluorination on the Properties of LiTFSI-Based Electrolytes for Li-Ion Batteries, *Electrochim. Acta*, 2015, **161**, 159–170, DOI: 10.1016/J.ELECTACTA.2015.02.042.

61 B. Ravikumar, M. Mynam and B. Rai, Effect of Salt Concentration on Properties of Lithium Ion Battery Electrolytes: A Molecular Dynamics Study, *J. Phys. Chem. C*, 2018, **122**(15), 8173–8181, DOI: 10.1021/acs.jpcc.8b02072.

62 C. Tian, K. Qin and L. Suo, Concentrated Electrolytes for Rechargeable Lithium Metal Batteries, *Mater. Futures*, 2023, **2**(1), 012101, DOI: 10.1088/2752-5724/acac68.

63 N. Bou-Rabee, Time Integrators for Molecular Dynamics, *Entropy*, 2013, **16**(1), 138–162, DOI: 10.3390/e16010138.

64 Y. Lin, D. Pan, J. Li, L. Zhang and X. Shao, Application of Berendsen Barostat in Dissipative Particle Dynamics for Nonequilibrium Dynamic Simulation, *J. Chem. Phys.*, 2017, **146**(12), 124108, DOI: 10.1063/1.4978807.

65 B. Hess, H. Bekker, H. J. C. Berendsen and J. G. E. M. Fraaije, LINCS: A Linear Constraint Solver for Molecular Simulations, *J. Comput. Chem.*, 1998, **18**(12), 1463–1472.

66 W. F. Van Gunsteren and H. J. C. Berendsen, A Leap-Frog Algorithm for Stochastic Dynamics, *Mol. Simul.*, 1988, **1**(3), 173–185, DOI: 10.1080/08927028808080941.

67 P. Wróbel, P. Kubisiak and A. Eilmes, MeTFSI (Me = Li, Na) Solvation in Ethylene Carbonate and Fluorinated Ethylene Carbonate: A Molecular Dynamics Study, *J. Phys. Chem. B*, 2021, **125**(4), 1248–1258, DOI: 10.1021/ACS.JPCB.0C10622.

68 D. A. Rakov, F. Chen, S. A. Ferdousi, H. Li, T. Pathirana, A. N. Simonov, P. C. Howlett, R. Atkin and M. Forsyth, Engineering High-Energy-Density Sodium Battery Anodes for Improved Cycling with Superconcentrated Ionic-Liquid

Electrolytes, *Nat. Mater.*, 2020, **19**(10), 1096–1101, DOI: 10.1038/s41563-020-0673-0.

69 M. Chintapalli, T. N. P. Le, N. R. Venkatesan, N. G. Mackay, A. A. Rojas, J. L. Thelen, X. C. Chen, D. Devaux and N. P. Balsara, Structure and Ionic Conductivity of Polystyrene-*Block*-Poly(Ethylene Oxide) Electrolytes in the High Salt Concentration Limit, *Macromolecules*, 2016, **49**(5), 1770–1780, DOI: 10.1021/acs.macromol.5b02620.

70 A. France-Lanord and J. C. Grossman, Correlations from Ion Pairing and the Nernst-Einstein Equation, *Phys. Rev. Lett.*, 2019, **122**(13), 136001, DOI: 10.1103/PHYSREVLETT.122.136001.

71 B. Ma, T. D. Nguyen and M. Olvera de la Cruz, Control of Ionic Mobility via Charge Size Asymmetry in Random Ionomers, *Nano Lett.*, 2020, **20**(1), 43–49, DOI: 10.1021/acs.nanolett.9b02743.

72 J. R. Keith, N. J. Rebello, B. J. Cowen and V. Ganesan, Influence of Counterion Structure on Conductivity of Polymerized Ionic Liquids, *ACS Macro Lett.*, 2019, **8**(4), 387–392, DOI: 10.1021/ACSMACROLETT.9B00070.

73 A. Kisliuk, V. Bocharova, I. Popov, C. Gainaru and A. P. Sokolov, Fundamental Parameters Governing Ion Conductivity in Polymer Electrolytes, *Electrochim. Acta*, 2019, **299**, 191–196, DOI: 10.1016/J.ELECTACTA.2018.12.143.

74 J. R. Sangoro, C. Iacob, A. L. Agapov, Y. Wang, S. Berdzinski, H. Rexhausen, V. Strehmel, C. Friedrich, A. P. Sokolov and F. Kremer, Decoupling of Ionic Conductivity from Structural Dynamics in Polymerized Ionic Liquids, *Soft Matter*, 2014, **10**(20), 3536–3540, DOI: 10.1039/C3SM53202J.

75 A. J. Ringsby, K. D. Fong, J. Self, H. K. Bergstrom, B. D. McCloskey and K. A. Persson, Transport Phenomena in Low Temperature Lithium-Ion Battery Electrolytes, *J. Electrochem. Soc.*, 2021, **168**(8), 080501, DOI: 10.1149/1945-7111/AC1735.

76 A. Maitra and A. Heuer, Cation Transport in Polymer Electrolytes: A Microscopic Approach, *Phys. Rev. Lett.*, 2007, **98**(22), 227802, DOI: 10.1103/PHYSREVLETT.98.227802.

77 M. Fischer, A. Heuer and D. Diddens, Structure and Transport Properties of Poly(Ethylene Oxide)-Based Cross-Linked Polymer Electrolytes-A Molecular Dynamics Simulations Study, *Macromolecules*, 2022, **55**(22), 10229–10242, DOI: 10.1021/ACS.MACROMOL.2C01795.

78 M. Mouas, J.-G. Gasser, S. Hellal, B. Grosdidier, A. Makradi and S. Belouettar, Diffusion and Viscosity of Liquid Tin: Green-Kubo Relationship-Based Calculations from Molecular Dynamics Simulations, *J. Chem. Phys.*, 2012, **136**(9), 094501, DOI: 10.1063/1.3687243.

79 T. Chen, B. Smit and A. T. Bell, Are Pressure Fluctuation-Based Equilibrium Methods Really Worse than Nonequilibrium Methods for Calculating Viscosities?, *J. Chem. Phys.*, 2009, **131**(24), 246101, DOI: 10.1063/1.3274802.

80 B. Hess, Determining the Shear Viscosity of Model Liquids from Molecular Dynamics Simulations, *J. Chem. Phys.*, 2001, **116**(1), 209, DOI: 10.1063/1.1421362.

81 J. C. F. Schulz, A. Schlaich, M. Heyden, R. R. Netz and J. Kappler, Molecular Interpretation of the Non-Newtonian Viscoelastic Behavior of Liquid Water at High Frequencies, *Phys. Rev. Fluids*, 2020, **5**(10), 103301, DOI: 10.1103/PhysRevFluids.5.103301.

82 E. R. Logan, E. M. Tonita, K. L. Gering, L. Ma, M. K. G. Bauer, J. Li, L. Y. Beaulieu and J. R. Dahn, A Study of the Transport Properties of Ethylene Carbonate-Free Li Electrolytes, *J. Electrochem. Soc.*, 2018, **165**(3), A705–A716, DOI: 10.1149/2.0981803jes.

83 K. Hayamizu, Y. Aihara, S. Arai and C. G. Martinez, Pulse-Gradient Spin-Echo ^{1}H, ^{7}Li, and ^{19}F NMR Diffusion and Ionic Conductivity Measurements of 14 Organic Electrolytes Containing $LiN(SO_2CF_3)_2$, *J. Phys. Chem. B*, 1999, **103**(3), 519–524, DOI: 10.1021/JP9825664.

84 B. L. Bhargava and S. Balasubramanian, Refined Potential Model for Atomistic Simulations of Ionic Liquid [Bmim][PF_6], *J. Chem. Phys.*, 2007, **127**(11), 114510, DOI: 10.1063/1.2772268.

85 Y. Zhang and E. J. Maginn, Direct Correlation between Ionic Liquid Transport Properties and Ion Pair Lifetimes: A Molecular Dynamics Study, *J. Phys. Chem. Lett.*, 2015, **6**(4), 700–705, DOI: 10.1021/ACS.JPCLETT.5B00003.

86 O. Borodin and G. D. Smith, Structure and Dynamics of N-Methyl-N-Propylpyrrolidinium Bis(Trifluoromethanesulfonyl)Imide Ionic Liquid from Molecular Dynamics Simulations, *J. Phys. Chem. B*, 2006, **110**(23), 11481–11490, DOI: 10.1021/JP061593O.

87 S. Mogurampelly and V. Ganesan, Effect of Nanoparticles on Ion Transport in Polymer Electrolytes, *Macromolecules*, 2015, **48**(8), 2773–2786, DOI: 10.1021/MA502578S.

88 J. R. Keith, S. Mogurampelly, F. Aldukhi, B. K. Wheatle and V. Ganesan, Influence of Molecular Weight on Ion-Transport Properties of Polymeric Ionic Liquids, *Phys. Chem. Chem. Phys.*, 2017, **19**(43), 29134–29145, DOI: 10.1039/C7CP05489K.

89 F. Fan, Y. Wang, T. Hong, M. F. Heres, T. Saito and A. P. Sokolov, Ion Conduction in Polymerized Ionic Liquids with Different Pendant Groups, *Macromolecules*, 2015, **48**(13), 4461–4470, DOI: 10.1021/acs.macromol.5b00257.

90 J. L. Plawsky, *Transport Phenomena Fundamentals*, Series: Chemical industries, CRC Press, Boca Raton, 4th edn, 2020. DOI: 10.1201/9781315113388.

91 O. Borodin and G. D. Smith, LiTFSI Structure and Transport in Ethylene Carbonate from Molecular Dynamics Simulations, *J. Phys. Chem. B*, 2006, **110**(10), 4971–4977, DOI: 10.1021/jp056249q.

92 H. Tokuda, S. Muto, N. Hoshi, T. Minakata, M. Ikeda, F. Yamamoto and M. Watanabe, Synthesis, Characterization, and Ion-Conductive Behavior in an Organic Solvent and in a Polyether of a Novel Lithium Salt of a Perfluorinated Polyimide Anion, *Macromolecules*, 2002, **35**(4), 1403–1411, DOI: 10.1021/ma011904n.

93 S. Mohapatra, S. Halder, S. R. Chaudhari, R. R. Netz and S. Mogurampelly, Insights into the Structure and Ion Transport of Pectin-[BMIM][PF_6] Electrolytes, *J. Chem. Phys.*, 2023, **159**(15), 154902, DOI: 10.1063/5.0158127.

94 D. J. Brooks, B. V. Merinov, W. A. Goddard, B. Kozinsky and J. Mailoa, Atomistic Description of Ionic Diffusion in PEO-LiTFSI: Effect of Temperature, Molecular Weight, and Ionic Concentration, *Macromolecules*, 2018, **51**(21), 8987–8995, DOI: **10.1021/ACS.MACROMOL.8B01753**.

95 W. Gorecki, M. Jeannin, E. Belorizky, C. Roux and M. Armand, Physical Properties of Solid Polymer Electrolyte PEO(LiTFSI) Complexes, *J. Phys.: Condens. Matter*, 1995, **7**(34), 6823–6832, DOI: **10.1088/0953-8984/7/34/007**.

96 D. Devaux, R. Bouchet, D. Glé and R. Denoyel, Mechanism of Ion Transport in PEO/LiTFSI Complexes: Effect of Temperature, Molecular Weight and End Groups, *Solid State Ionics*, 2012, **227**, 119–127, DOI: **10.1016/J.SSI.2012.09.020**.

97 K. Hayamizu, E. Akiba, T. Bando and Y. Aihara, ^{1}H, ^{7}Li, and ^{19}F Nuclear Magnetic Resonance and Ionic Conductivity Studies for Liquid Electrolytes Composed of Glymes and Polyetheneglycol Dimethyl Ethers of $CH_3O(CH_2CH_2O)NCH_3$ (N = 3–50) Doped with $LiN(SO_2CF_3)_2$, *J. Chem. Phys.*, 2002, **117**(12), 5929, DOI: **10.1063/1.1501279**.